Volume 1 | Number 1 | Jan 2013 | Pages 1–100

Journal of
Materials Chemistry A

Materials for energy and sustainability
www.rsc.org/materialsA

ROYAL SOCIETY
OF CHEMISTRY

www.rsc.org/materialsA

1　Template-free Method towards Quadrate Co$_3$O$_4$ Nanoboxes from Cobalt

2　Coordination Polymer Nano-solids for High Performance Lithium Ion Battery

3　Anodes

4　　　　　　　　　　　Huawei Song, Lisha Shen, and Chengxin Wang [*]

5　State Key Laboratory of Optoelectronic Materials and Technologies, School of Physics Science and

6　Engineering, Sun Yat-sen (Zhongshan) University, Guangzhou 510275, People's Republic of China

* Address correspondence to wchengx@mail.sysu.edu.cn, Tel & Fax: +86-20-84113901

Abstract

Transition metal oxide hollow architectures are intensive explored for energy conversion and storage application. Feasible strategies towards various hollow architectures, particular those with non-spherical skeleton, are especially attracted. Quadrate Co_3O_4 nanoboxes are fabricated through controlled annealing of cobalt coordination polymer nano-solids with tunable dimensions. The cobalt coordination polymer in quadrate wires, cuboids, cubes is synthesized by temperature and concentration dependent solvothermal method. The nanoboxes' evolution involves Co_3O_4 shell's formation and uniformly depletion of cobalt coordination polymer in the core. Benefiting from the well-defined hollow interior and nanosized crystals, those quadrate nanoboxes have large specific surface and abundant hierarchical pores. When evaluated as anode materials for Lithium ion batteries, those boxes exhibited excellent electrochemical properties. Besides superior storage capability of 1200 mAhg^{-1} at 0.2 Ag^{-1}, the remarkable retention of 625 mAhg^{-1} at large rate of 10 Ag^{-1} is also obtained in the meantime.

Keywords: cobalt coordination polymer●Co_3O_4● quadrate nanobox●adjustable dimensions●Lithium ion battery

Introduction

Recent years have witnessed the rise of various hollow micro/nano architectures.[1-5] Due to high hierarchical porosity and large specific surface, those hollow structures are potentially attracted in catalysis, sensing, lithium-ion batteries and supercapacitors for easy surface permeability, fast transport, and compatible host-guest chemistry.[6-10] Generally speaking, the approach to hollow structures can be of template or non-template. For the template method, various templates with well-defined morphology and suitable dimensions are essential except for tedious template etching post treatment.[11-13] For example, Yu et al. have prepared a family of one dimensional inorganic nanotubes templated by carbon nanofibres.[14, 15]Moreover, various hollow spheres are prepared by using silica template.[16, 17] Recently, more and more non-template methods such as self-assembly of

1   nanoparticles, thermal oxidation, Kirkendall effect, galvanic replacement, and Ostwald ripening are

2   developed.[18-24] The feasibility of those strategies commonly lies in the disparity of physicochemical stability

3   and reactivity between involved components.

4   Coordination polymers assembled by metal ions and organic ligands exhibit excellent designability and

5   versatility in fabricating various architectures as spheres, quadrate wires, cuboids, cubes, and other

6   polyhedrons.[25-36] Hence, tailoring coordination polymers to obtain metal oxide hollow architectures, especially

7   some non-spherical ones with high curvature surface, is promising for many functional nanomaterials. For

8   example, Oh and coworkers achieved various In_2O_3 hollow structures and ball-in-ball hybrid oxides through

9   calcination of Indium coordination polymers and cations exchange reaction.[27, 29] Low and coworkers fabricated

10 Fe_2O_3 microboxes by annealing Prussian blue microcubes.[30] ZnS hollow polyhedrons were synthesized by Chen

11 and coworkers with ZIF-8.[28] Although significant development has been achieved, the new emerging field is

12 still full of vigor and vitality. Not to mention the design of novel coordination polymers, the modification of

13 existing ones and the phenomena in their transformation would exhibit variations. The search of scalable,

14 morphology and dimensions adjustable coordination polymers and the disclosing of something behind their

15 controllable transformation to various hollow structures are still highly desired.

16   As one of the candidates for conversion type electrode materials, Co_3O_4 perform as $Co_3O_4 + 8Li^+ + 8e^- \rightleftarrows$

17 $3Co + 4Li_2O$ in lithium ion batteries anode corresponding to a theoretical capacity about three times larger than

18 graphite.[37, 38] Due to robust structures, large specific surface, relative high charge/discharge voltage and small

19 active materials, novel Co_3O_4 hollow architectures exhibit high capacity, excellent cycling performance, and

20 improved safety during batteries operation. Despite relative low initial coulombic efficiency and volumetric

21 energy density, novel Co_3O_4 hollow architectures would be still highly desired in case the relative lower

22 coulombic efficiency and volumetric energy density are partly overcome by prelithiation treatment and superior

23 storage capability and high active materials loading on each electrode.

1 Herein, we present the controllable synthesis of a cobalt coordination polymer into quadrate wires, cuboids,

2 cubes with varying dimensions. Through mild annealing, those cobalt coordination polymer naono-solids are

3 transformed into Co_3O_4 quadrate tubular nanoboxes (QTNBs), rectangular nanoboxes (RNBs), cubic nanoboxes

4 (CNBs) of different size respectively. When evaluated as anodes for Lithium ion batteries, those nanoboxes

5 manifested superior storage capability and excellent rate capability.

6 **Experimental**

7 **Cobalt Coordination Polymer Nano-solids and Co_3O_4 Nanoboxes Synthesis**. All the reagents were used

8 after purchase and without purification. Quadrate nanoarchitectures of cobalt coordination polymer in wires,

9 cuboids, and cubes are fabricated by a modified solvothermal method. The length and width of the wires,

10 cuboids and cubes can be adjusted by altering the temperature and the concentration of cobalt acetate. To obtain

11 the wires, 0.004 M cobalt acetate hydrate (Alfa Aesar, AR) ethanol solvent is solvothermally treated at 60 ^{o}C

12 for 2 h, while the cuboids can be achieved with 0.008 M cobalt acetate at 90 ^{o}C for 2h and the cubes with 0.1 M

13 cobalt acetate at 120 ^{o}C for 0.5 h. All the reaction was performed in teflon-lined stainless steel autoclaves (50

14 mL) with the filling rate of 60%. To get the related boxes, the cobalt coordination polymer is mildly annealed in

15 flowing air. Typically, the QTNBs, RNBs, and CNBs are achieved through annealing the cobalt coordination

16 polymer at 200 ^{o}C for 6 hours.

17 **Physiochemical characterization**. Morphologies of the samples were characterized by a thermal field

18 emmission scanning electron microscope (SEM) (Quanta 400F) under 20 kV and a transmission electron

19 microscope (TEM) (FEI Tecnai G2 F30) under 300 kV. Structures, composition and elemental analysis were

20 performed by X-ray diffraction (XRD) (D/MAX 2200 VPC), energy dispersive spectroscopy (EDS), and

21 scanning transmission electron microscopy (STEM) mounted on the SEM and TEM. The surface area and pore

22 analysis were carried out on a Micromeritics instrument (ASAP 2420) with N_2 as absorbate at 77 K. The

1   Specific surface area and pore distribution were evaluated based on Brunauer-Emmett-Teller (BET) specific

2   surface and Barrett-Joyner-Halenda (BJH) desorption pore.

3   **Cells Fabrication and Tests**. For electrochemical characterization, the cobalt oxide nanoboxes (QTNBs,

4   RNBs, or CNBs), acetylene black and polyvinylidene fluoride with a weight ratio of 70:20:10 were mixed with

5   a small amount of 1-Methyl-2-pyrrolidinone (NMP) to forming a slurry mixture. The electrodes were fabricated

6   by pasting the slurry mixture on copper foil by an automatic thick film coater (AFA-I). Then the coating film

7   was desiccated in an vacuum chamber at 90 ^{o}C for 12 h. After that the foil is pressed by an electromotive roller

8   (MR-100A) and tailored to appropriate size by a coin-type cell microtome (T-06) (S=1.5 cm^2). The loadage of

9   active materials (1.2~ 1.5 mg) on each piece was determined by a microbalance (d=0.1 μg). Standard cells

10   (CR2032) with the above tailored foils as working electrode and lithium foils as the reference and counter

11   electrode, polypropylene micromembrane (Clegard 2500) as the separator, 1M LiPF$_6$ in ethylene carbonate

12   (EC) and diethyl carbonate (DEC) with a weight ratio of 1:1 as the electrolyte, were assembled in an Ar-filled

13   universal glove box with the Oxygen and water vapor pressure less than 0.3 ppm. The Cyclic voltammograms

14   (CVs) scanning at 0.2 mV s^{-1} in a voltage window of 0-3 V and electrochemical impedance spectroscopy (EIS)

15   scanning from 100 kHz to 0.1 Hz with an ac signal amplitude of 10 mV were both carried out on an Ivium

16   electrochemical workstation. For cycling and rate performance, the cells were galvanostatically charged and

17   discharged in a volatage cutoff of 0.005-3 V at various rates on a mulitichannel Neware battery testing system.

18   **Results and discussion**

19   To synthesize the cobalt coordination polymer nano-solids, a modified solvothermal method is adopted.[39, 40]

20   By altering the concentration of cobalt acetate and reaction temperature, quadrate nanoarchitectures in wires,

21   cuboids, and cubes are fabricated. The length and width of the wires, cuboids and cubes can be well adjusted.

22   Figure 1(a) shows the cobalt coordination polymer wires have fairly uniformed dimensions of several

23   micrometers long. The magnified SEM image (Figure 1(b)) reveals the wires all have quadrate configurations

1   with width about 100 nm. The even contrast in the TEM image (Figure 1(c)) indicates the solid construction of

2   those wires. Similarly, the cobalt coordination polymer cuboids and cubes are presented in Figure 1(d)-(f) and

3   Figure 1(g)-(i) respectively. They also exhibit quadrate configurations and solid constructions as those

4   nanowires except different dimensions.

5   Those cobalt coordination polymer nano-solids were further verified as $Co_5(OH)_2(O_2CCH_3)_8 \cdot 2H_2O$ with a

6   tetragonal symmetry (Space group: $I4_1/a$, a=b=23.693(2) Å, c=11.565 (5) Å, $\alpha=\beta=\gamma=90$ ^oC).[39] Figure 2(a)

7   exhibits XRD patterns of the as-prepared cobalt coordination polymer nano-solids in comparison with the

8   simulated one for $Co_5(OH)_2(O_2CCH_3)_8 \cdot 2H_2O$. The well consistent peaks indicate the phase pure of the as-

9   prepared cobalt coordination polymers. To obtain the relevant transition metal oxide nanoboxes, those

10   coordination polymer nano-solids are calcinated. By evaluation of the products annealed at different

11   temperature, a mild annealing process of 200 ^oC and 6 hours is essential for the totally conversion from cobalt

12   coordination polymer to cobalt oxide (Figure 2(b)). The XRD pattern of the as-prepared cobalt coordination

13   polymer solids annealed at 200 ^oC for 6 hours is well consistent with cubic Co_3O_4 (PDF No. 42-1467; space

14   group: Fd-3m, a=b=c=8.0837 Å, $\alpha=\beta=\gamma=90$ ^oC). No additional diffraction peaks from impurities were detected,

15   indicating the cobalt coordination polymer is all transformed into Co_3O_4. The corresponding EDX spectra

16   (Figure 2(c)) also verify the disappearance of cobalt coordination polymer after annealing. Moreover, the

17   morphology modification (Figure 2(d)) of the solid wires annealed for different durations reveals the

18   transformation from cobalt coordination polymer to cobalt oxide involves the formation of quadrate tubular

19   shell probably Co_3O_4 and the uniformly depletion of coordination polymer core, finally resulting in the non-

20   spherical quadrate tubular Co_3O_4 nanoboxes. The mechanism involves oxidative decomposition of the cobalt

21   coordination polymer and the formation of the Co_3O_4 shell well consistent with other reported hollow

22   counterparts.[30, 33, 41]

1   The as-prepared QTNBs, RNBs, CNBs in different size could be achieved from the annealing of the relevant

2   cobalt coordination polymer nano-solids shown in Figure 1. To exemplify the hollow architectures in detail,

3   each of those QTNBs, RNBs, and CNBs are presented. Figure 3 exhibits the SEM, STEM and TEM images of

4   the QTNBs, RNBs, and CNBs respectively. The QTNBs have a length of several micrometers and a width of a

5   few tens nanometers. The length decreases to about one micrometer scale for RNBs. As to the CNBs, the

6   quadrate architectures almost emerge as well-defined cubic skeleton in several hundred nanometers. The

7   corresponding STEM and TEM images show well-defined quadrate hollow interior and the mapping images

8   depict well distribution of Co and O in those unique nanoboxes. Therefore, controllable dimensions in quadrate

9   hollow transition metal oxide nanostructures are readily realized by mild annealing of their coordination

10   polymer. The SAED images (Figure 4(a)-(c)) verify the exclusive existence of phase-pure Co_3O_4 (PDF No. 42-

11   1467) for QTNBs, RNBs, and CNBs respectively well consistent with those depicted in the XRD patterns.

12   Moreover, the nanoparticles in the porous skeleton are further confirmed as nanocrystals smaller than 10 nm

13   with well-defined lattice fringes ascribed to characteristic planes of Co_3O_4 (PDF No. 42-1467) in the HRTEM

14   images (Figure 4(d)-(f)). Figure 5(a) presents the adsorption and desorption isotherms for the different

15   nanoboxes. They show similar type III isotherms.[42, 43] Based on the isotherms, BET surface areas of 62.5 m^2g^{-1},

16   51.4 m^2g^{-1}, and 34.4 m^2g^{-1} are attained for QTNBs, RNBs, and CNBs respectively. The non-closed isotherm for

17   QTNBs is probably resulted from the desorption hysteresis of abundant mesopores.[44] BJH pore distribution

18   (Figure 5(b)) depict their hierarchal pore distribution with accumulated desorption pore volume of 0.25, 0.20,

19   and 0.11 cm^3g^{-1} respectively (Pore diameter from 1.7 nm to 300 nm).

20   The electrochemical evaluation is presented in Figure 6. The typical charge-discharge curves (Figure 6(a))

21   depict QTNBs, RNBs, and CNBs deliver initial capacity of 1447, 1376, and 1353 $mAhg^{-1}$ respectively. In

22   comparison with the charging capacity, irreversible capacity of 222, 252, 344 $mAhg^{-1}$ fades respectively due to

23   formation of solid electrolyte interphase (SEI) layers. The long plateaus about 1 V in the discharging and those

24   near 2 V in the charging are well consistent with previous reports attributing to reduction of Co_3O_4 to Co and

1   reformation of Co_3O_4 based on the mentioned conversion reaction ($Co_3O_4+8Li^++8e^- \rightleftarrows 3Co+4Li_2O$).[45-49] This

2   transformation corresponds well to the CV results (Figure 6(b)) with marked hysteresis as most conversion type

3   electrodes.[50-56] The redox peaks shift to lower voltage from CNBs to QTNBs is probably attributed to easier ion

4   accessibility and relevant weakened hysteresis which are also reflected in the following higher initial coulombic

5   efficiency and faster kinetic processes (Figure 6 (c)-(f)). To evaluate the cycling performance, the various

6   nanoboxes are tested at 0.5 Ag^{-1} over the voltage range of 0.005-3V (Figure 6(c)). Comparing with Co_3O_4

7   nanoparticles and other counterparts, these nanoboxes all exhibit more excellent lithium ion storage and cycling

8   capability without capacity fading for 50 cycles.[37, 56-59] The increase for cycling capacities is common for much

9   transition metal oxide due to increasing interfaces.[60, 61] Moreover, the efficiencies ((Figure 6(d))) near 96% were

10   retained from the second cycle. The improved cycling capability and efficiency probably relate to the large

11   specific surface and abundant hierarchical pores. Besides well cycling performance, those electrodes also

12   exhibit excellent rate capability when tested at altering rates from 0.2 Ag^{-1} to 10 Ag^{-1}(Figure 6(e)). In particular,

13   the QTNBs retain capacity of 1240 $mAhg^{-1}$ at 0.2 Ag^{-1}, 1013 $mAhg^{-1}$ at 1 Ag^{-1}, 834 $mAhg^{-1}$ at 5 Ag^{-1}, and 625

14    $mAhg^{-1}$ at 10 Ag^{-1}. From CNBs to QTNBs, remarkable improvement in cycling performance, rate performance,

15   and efficiencies at different rates are realized in the meantime (Figure 6(c)-(f)). The improvement is probably

16   not only dependent on the increasing BET surface and BJH pores, but also on the easily accessing of ions and

17   electrons resulted from the well-defined hollow structures.

18   To further illustrate the robust structures and fast kinetic processes. Ex-situ SEM images for the cycled

19   electrode and the EIS plots are presented in Figure 7. As shown in Figure 7 (a)-(c), the various nanoboxes still

20   retain their initial hollow skeletons after 50 cycles despite marked deformation resulted from lithiation-

21   delithiation processes. This reveals the robust structural stability of those nanoboxes. The Nyquist plots of the

22   precycled nanoboxes are characteristic of a squashed semicircle in the high-frequency region and a quasi-

23   sloping line in the low-frequency region ascribing charge transferring resistance (Rct) and the Warburg

1   impedance (Rw) relevant to solid-state diffusion respectively. Evidently, the Rct for QTNBs is lower than those

2   of RNBs and CNBs (~130 ohm vs. ~230 ohm, ~250 ohm). This is well consistent with the superior rate

3   performance for QTNBs comparing with RNBs and CNBs revealing faster kinetic processes and easier ion

4   accessibility in QTNBs. After 50 cycles, the semicircle in the high-frequency region is replaced by two smaller

5   semicircles in the high-frequency region and the mid-frequency region. As shown in the equivalent circuit, the

6   former semicircle relates to the resistance of SEI (Rs), while the latter still reflects the Rct of electrode materials.

7   The lowered Rct (~10 ohm vs.130 ohm for QTNBs; ~10 ohm vs. 230 ohm for RNBs; ~60 ohm vs. 250 ohm for

8   CNBs) implies charging transferring processes are significantly improved due to fast ion conductivity in the SEI

9   and active materials after successive lithiation and de-lithiation. The almost same electrolyte resistance (Re)

10   indicates the well stability of electrolyte. The improvement in kinetics processes and ion storage capability

11   manifested the advantage of controlled annealing of coordination polymer over other strategies in controllable

12   operation between electrochemical properties and microstructures (morphology, phase, and dimensions).

13   **Conclusions**

14   We have demonstrated the well feasibility to improve electrochemical properties by altering microstructures

15   in quadrate Co_3O_4 nanoboxes. Through a facile solvothermal method, controllable dimensions in a cobalt

16   coordination polymer are realized in various quadrate wires, cuboids and cubes. By mild annealing process, that

17   solid coordination polymer is transformed into relevant nanoboxes. The transformation process involving

18   transition metal oxide shell formation and further depletion of coordination polymer in the core is verified.

19   Those nanoboxes exhibit superior storage capability, excellent cycling and rate performance. For coordination

20   chemistry, the traditional fields of designing coordination polymer and their direct application have gone

21   through the spring stage. The downward of tailoring coordination polymer and their controlled annealing may

22   inject new vitality in the fascinating discipline by inspiring various applications of those novel architectures.

1   *Conflict of Interest*: The authors declare no competing financial interest.

4   **References**

5   1.   J. C. Groen, T. Bach, U. Ziese, A. M. Paulaime-van Donk, K. P. de Jong, J. A. Moulijn and J. Pérez-
6   Ramírez, *J. Am. Chem. Soc.*, 2005, **127**, 10792-10793.
7   2.   J. Bao, Y. Liang, Z. Xu and L. Si, *Adv. Mater.*, 2003, **15**, 1832-1835.
8   3.   M. M. Titirici, M. Antonietti and A. Thomas, *Chem. Mater.*, 2006, **18**, 3808-3812.
9   4.   K. An, S. G. Kwon, M. Park, H. B. Na, S. I. Baik, J. H. Yu, D. Kim, J. S. Son, Y. W. Kim, I. C. Song,
10   W. K. Moon, H. M. Park and T. Hyeon, *Nano Lett.*, 2008, **8**, 4252-4258.
11   5.   X. W. Lou, L. A. Archer and Z. Yang, *Adv. Mater.*, 2008, **20**, 3987-4019.
12   6.   C. J. Martinez, B. Hockey, C. B. Montgomery and S. Semancik, *Langmuir*, 2005, **21**, 7937-7944.
13   7.   C. Z. Wu, Y. Xie, L. Y. Lei, S. Q. Hu and C. Z. OuYang, *Adv. Mater.*, 2006, **18**, 1727-1732.
14   8.   B. Koo, H. Xiong, M. D. Slater, V. B. Prakapenka, M. Balasubramanian, P. Podsiadlo, C. S. Johnson, T.
15   Rajh and E. V. Shevchenko, *Nano Lett.*, 2012, **12**, 2429-2435.
16   9.   Q. H. Wang, L. F. Jiao, H. M. Du, Y. C. Si, Y. J. Wang and H. T. Yuan, *J. Mater. Chem.*, 2012, **22**,
17   21387-21391.
18   10.   S. S. Li, H. P. Cong, P. Wang and S. H. Yu, *Nanoscale*, 2014, **6**, 7534-7541.
19   11.   C. Yan and D. Xue, *J. Phys. Chem. B*, 2006, **110**, 7102-7106.
20   12.   R. Yuan, X. Fu, X. Wang, P. Liu, L. Wu, Y. Xu, X. Wang and Z. Wang, *Chem. Mater.*, 2006, **18**, 4700-
21   4705.
22   13.   S. Ding, J. S. Chen, G. Qi, X. Duan, Z. Wang, E. P. Giannelis, L. A. Archer and X. W. Lou, *J. Am.
23   Chem. Soc.*, 2010, **133**, 21-23.
24   14.   J. Y. Gong, S. R. Guo, H. S. Qian, W. H. Xu and S. H. Yu, *J. Mater. Chem.*, 2009, **19**, 1037-1042.
25   15.   H. W. Liang, J. W. Liu, H. S. Qian and S. H. Yu, *Acc. Chem. Res.*, 2013, **46**, 1450-1461.
26   16.   Y. Chen, H. R. Chen and J. L. Shi, *Acc. Chem. Res.*, 2013, **47**, 125-137.
27   17.   H. Song, N. Li, H. Cui and C. Wang, *Nano Energy*, 2014, **4**, 81-87.
28   18.   J. Liu and D. Xue, *Adv. Mater.*, 2008, **20**, 2622-2627.
29   19.   B. Liu and H. C. Zeng, *Small*, 2005, **1**, 566-571.
30   20.   H. C. Zeng, *J. Mater. Chem.*, 2006, **16**, 649-662.
31   21.   J. G. Yu, H. Guo, S. A. Davis and S. Mann, *Adv. Funct. Mater.*, 2006, **16**, 2035-2041.
32   22.   H. G. Yang and H. C. Zeng, *Angew. Chem., Inter. Ed.*, 2004, **43**, 5930-5933.
33   23.   H. B. Yao, X. B. Li, S. Y. Ai and S. H. Yu, *Nano Res.*, 2010, **3**, 81-91.
34   24.   H. P. Cong and S. H. Yu, *Cryst. Growth Des.*, 2008, **9**, 210-217.
35   25.   A. Umemura, S. Diring, S. Furukawa, H. Uehara, T. Tsuruoka and S. Kitagawa, *J. Am. Chem. Soc.*,
36   2011, **133**, 15506-15513.
37   26.   W. Cho, H. J. Lee and M. Oh, *J. Am. Chem. Soc.*, 2008, **130**, 16943-16946.
38   27.   W. Cho, Y. H. Lee, H. J. Lee and M. Oh, *Chem. Commun.*, 2009, 4756-4758.
39   28.   Z. Jiang, H. Sun, Z. Qin, X. Jiao and D. Chen, *Chem. Commun.*, 2012, **48**, 3620-3622.
40   29.   W. Cho, Y. H. Lee, H. J. Lee and M. Oh, *Adv. Mater.*, 2011, **23**, 1720-1723.

1 30. L. Zhang, H. B. Wu, S. Madhavi, H. H. Hng and X. W. Lou, *J. Am. Chem. Soc.*, 2012, **134**, 17388-
2   17391.
3 31. S. Jung and M. Oh, *Angew. Chem., Inter. Ed.*, 2008, **47**, 2049-2051.
4 32. S. K. Nune, P. K. Thallapally, A. Dohnalkova, C. Wang, J. Liu and G. J. Exarhos, *Chem. Commun.*,
5   2010, **46**, 4878-4880.
6 33. S. Jung, W. Cho, H. J. Lee and M. Oh, *Angew. Chem., Inter. Ed.*, 2009, **48**, 1459-1462.
7 34. K. E. deKrafft, C. Wang and W. Lin, *Advanced Materials*, 2012, **24**, 2014-2018.
8 35. R. Kaminker, R. Popovitz-Biro and M. E. van der Boom, *Angew. Chem., Inter. Ed.*, 2011, **123**, 3282-
9   3284.
10 36. T. R. Cook, Y.-R. Zheng and P. J. Stang, *Chem. Rev.*, 2012, **113**, 734-777.
11 37. L. Zhan, S. Wang, L. X. Ding, Z. Li and H. Wang, *Electrochim. Acta*, 2014, **135**, 35-41.
12 38. C. C. Li, X. M. Yin, Q. H. Li, L. B. Chen and T. H. Wang, *Chem. – A Euro. J.*, 2011, **17**, 1596-1604.
13 39. R. Kuhlman, G. L. Schimek and J. W. Kolis, *Inorg. Chem.*, 1998, **38**, 194-196.
14 40. W. Du, R. Liu, Y. Jiang, Q. Lu, Y. Fan and F. Gao, *J. Power Sources*, 2013, **227**, 101-105.
15 41. C. Li, X. Yin, L. Chen, Q. Li and T. Wang, *Chem. – A Euro. J.*, 2010, **16**, 5215-5221.
16 42. S. Brunauer, P. H. Emmett and E. Teller, *J. Am. Chem. Soc.*, 1938, **60**, 309-319.
17 43. A. T. Hubbard, *Encyclopedia of surface and colloid science*, Marcel Dekker, Inc., Ney York, **2002**..
18 44. Y. Y. Huang, T. J. McCarthy and W. M. H. Sachtler, *Appl. Catal., A*, 1996, **148**, 135-154.
19 45. F. Cheng, Z. Tao, J. Liang and J. Chen, *Chem. Mater.*, 2007, **20**, 667-681.
20 46. Y. J. Fu, X. W. Li, X. L. Sun, X. H. Wang, D. Q. Liu and D. Y. He, *J. Mater. Chem.*, 2012, **22**, 17429-
21   17431.
22 47. H. Huang, W. Zhu, X. Tao, Y. Xia, Z. Yu, J. Fang, Y. Gan and W. Zhang, *ACS Appl. Mater. Interfaces*,
23   2012, **4**, 5974-5980.
24 48. L. M. Wang, B. Liu, S. H. Ran, H. T. Huang, X. F. Wang, B. Liang, D. Chen and G. Z. Shen, *J. Mater..*
25   *Chem.*, 2012, **22**, 23541-23546.
26 49. X. Xiao, X. Liu, H. Zhao, D. Chen, F. Liu, J. Xiang, Z. Hu and Y. Li, *Adv. Mater.*, 2012, **24**, 5762-5766.
27 50. W. Dreyer, J. Jamnik, C. Guhlke, R. Huth, J. Moskon and M. Gaberscek, *Nat. Mater.*, 2010, **9**, 448-453.
28 51. H. Song, G. Yang, H. Cui and C. Wang, *Nano Energy*, 2014, **3**, 16-25.
29 52. G. Yang, H. Song, H. Cui and C. Wang, *Nano Energy*, 2014, **5**, 9-19.
30 53. G. Yang, H. Cui, G. Yang and C. Wang, *ACS Nano*, 2014, **8**, 4474-4487.
31 54. H. Song, H. Cui and C. Wang, *ACS Appl. Mater. Interfaces*, 2014, **6**, 13765–13769.
32 55. L. Shen, H. Song, H. Cui, X. Wen, X. Wei and C. Wang, *CrystEngComm*, 2013, **15**, 9849-9854.
33 56. L. Shen and C. Wang, *Electrochim. Acta*, 2014, **133**, 16-22.
34 57. D. Ge, H. Geng, J. Wang, J. Zheng, Y. Pan, X. Cao and H. Gu, *Nanoscale*, 2014, **6**, 9689-9694.
35 58. G. Huang, S. Xu, S. Lu, L. Li and H. Sun, *Electrochim. Acta*, 2014, **135**, 420-427.
36 59. Y. Kim, J. H. Lee, S. Cho, Y. Kwon, I. In, J. Lee, N. H. You, E. Reichmanis, H. Ko, K. T. Lee, H. K.
37   Kwon, D. H. Ko, H. Yang and B. Park, *ACS Nano*, 2014, **8**, 6701-6712.
38 60. X. Xu, R. Cao, S. Jeong and J. Cho, *Nano Lett.*, 2012, **12**, 4988-4991.
39 61. Y. Sun, X. Hu, W. Luo and Y. Huang, *J. Mater. Chem.*, 2012, **22**, 13826.
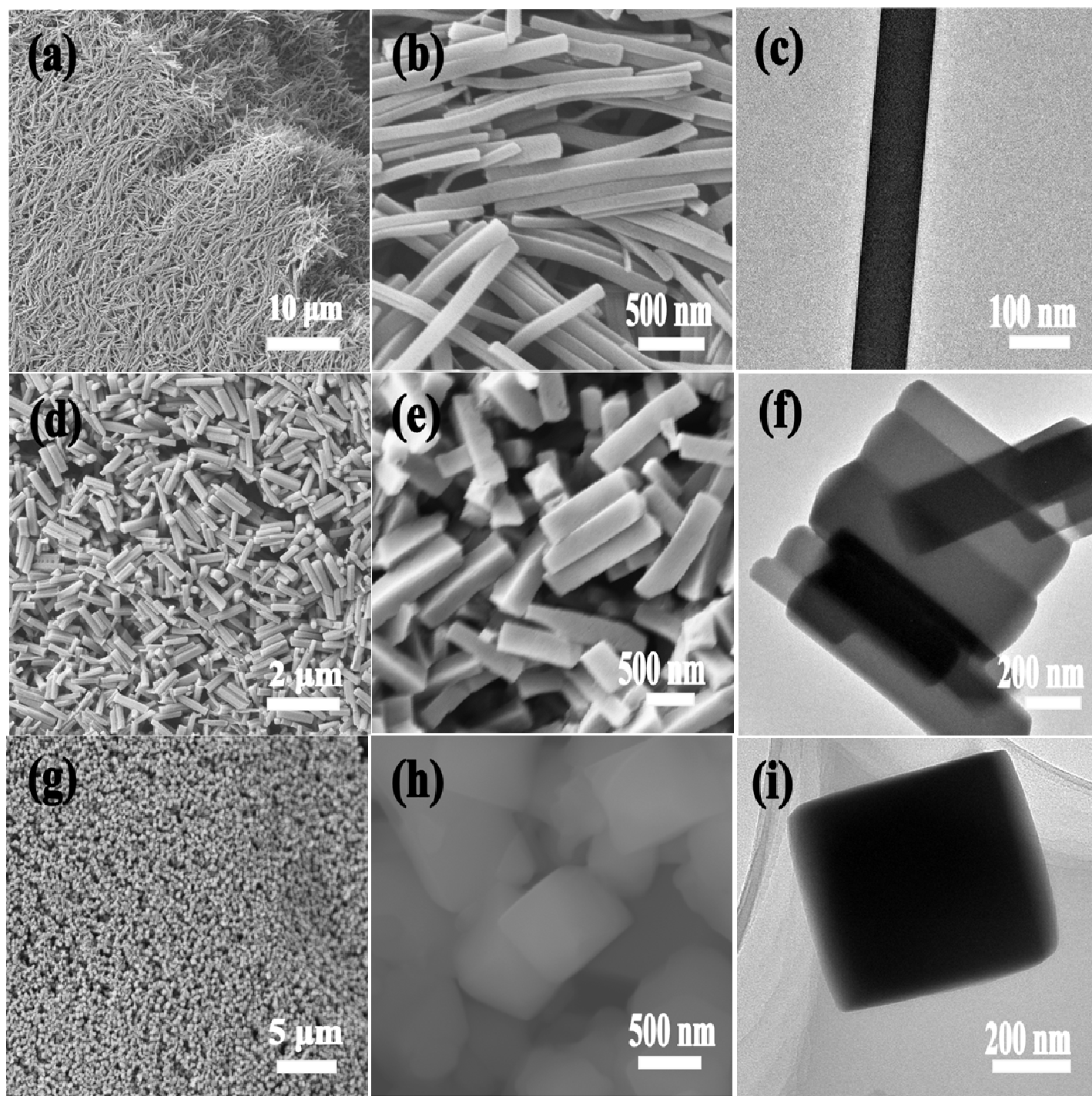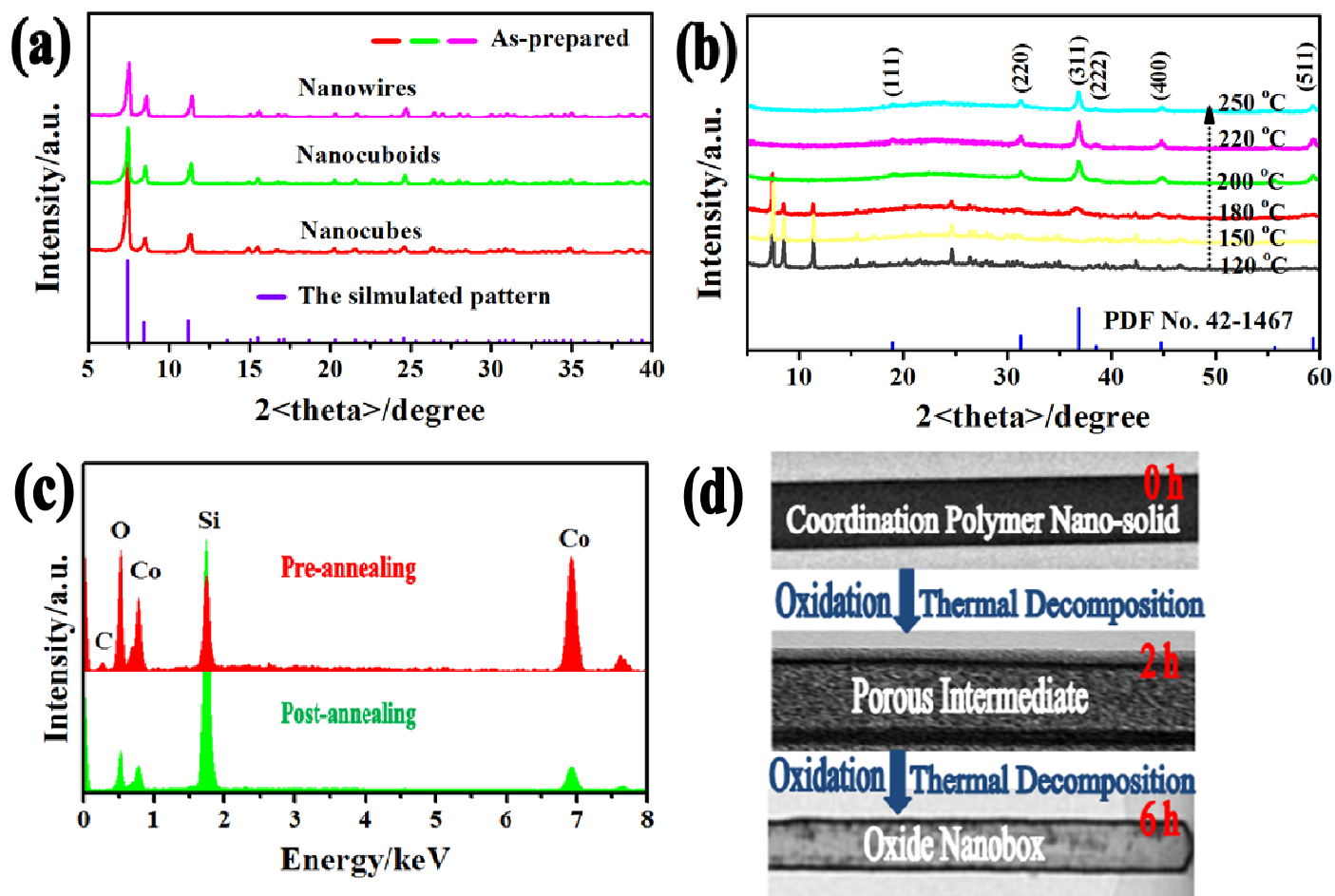40
41

42

Figure 1. SEM and corresponding TEM images for the cobalt coordination polymer nano-solids in (a)-(c) quadrate nanowires, (d)-(f) cuboids, and (g)-(i) cubes.

1

Figure 2. (a) XRD patterns for as-prepared cobalt coordination polymer nano-solids in comparison with the

simulated one according to literature.[31] (b) The phase evolution of cobalt coordination polymer nano-solids

(quadrate nanowires) annealing at different temperatures for 6 h in comparison with Co_3O_4 (PDF No. 42-1467).

(c) EDX spectra of cobalt coordination polymer nano-solids (quadrate nanowires) and the annealed product

(Annealing conditions: 200 ^{o}C for 6 h at ambient atmosphere). (d) Morphology modification of cobalt

coordination polymer nanosolids (quadrate nanowires) suffering from different durations at 200 ^{o}C.

8

1
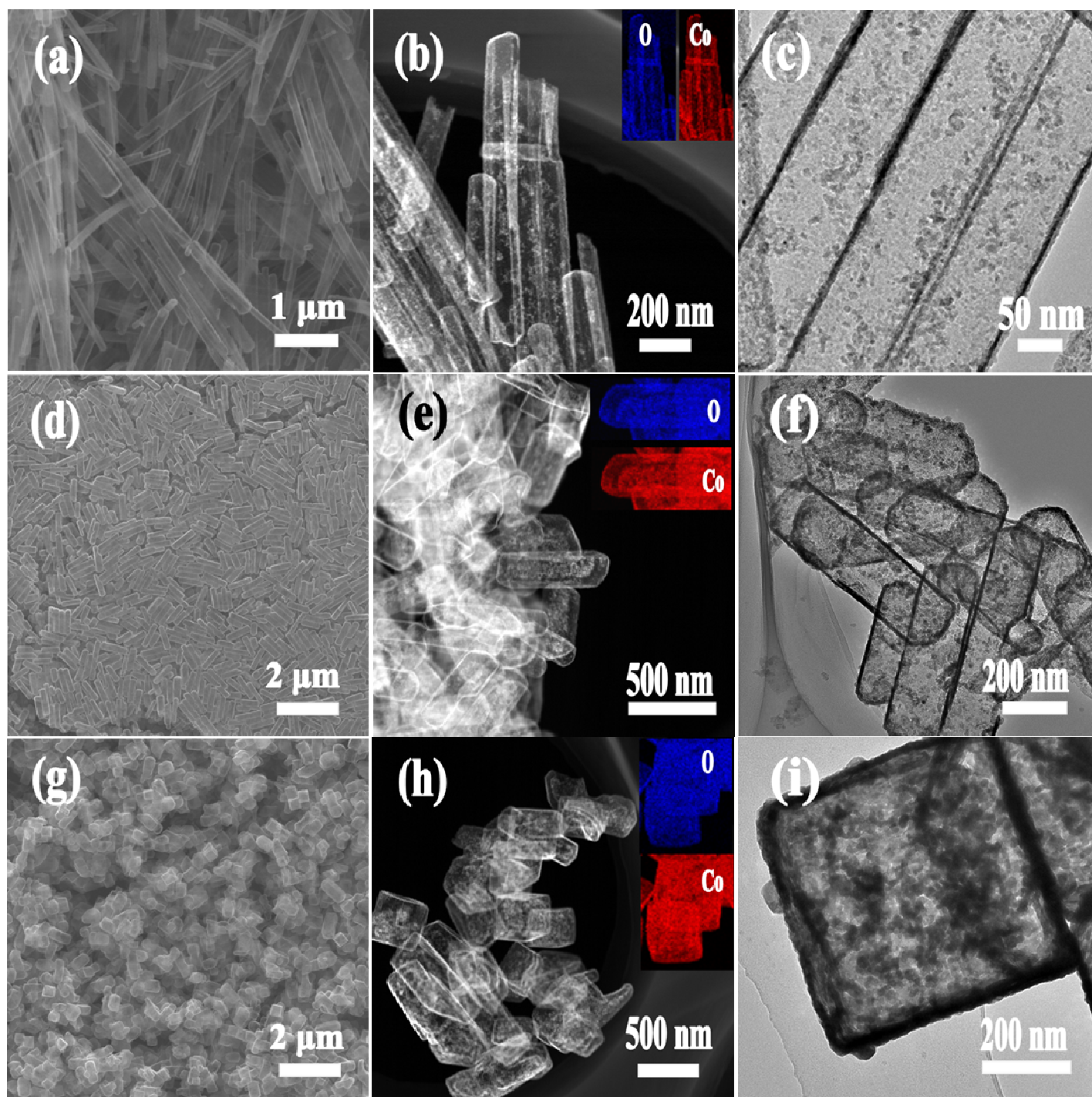
Figure 3. SEM, STEM, and TEM images for the cobalt coordination polymer nanosolids annealing at 200 °C

for 6 h at ambient atmosphere: (a)-(c) QTNBs, (d)-(f) RNBs, (g)-(i) CNBs, and inset views of the STEM images
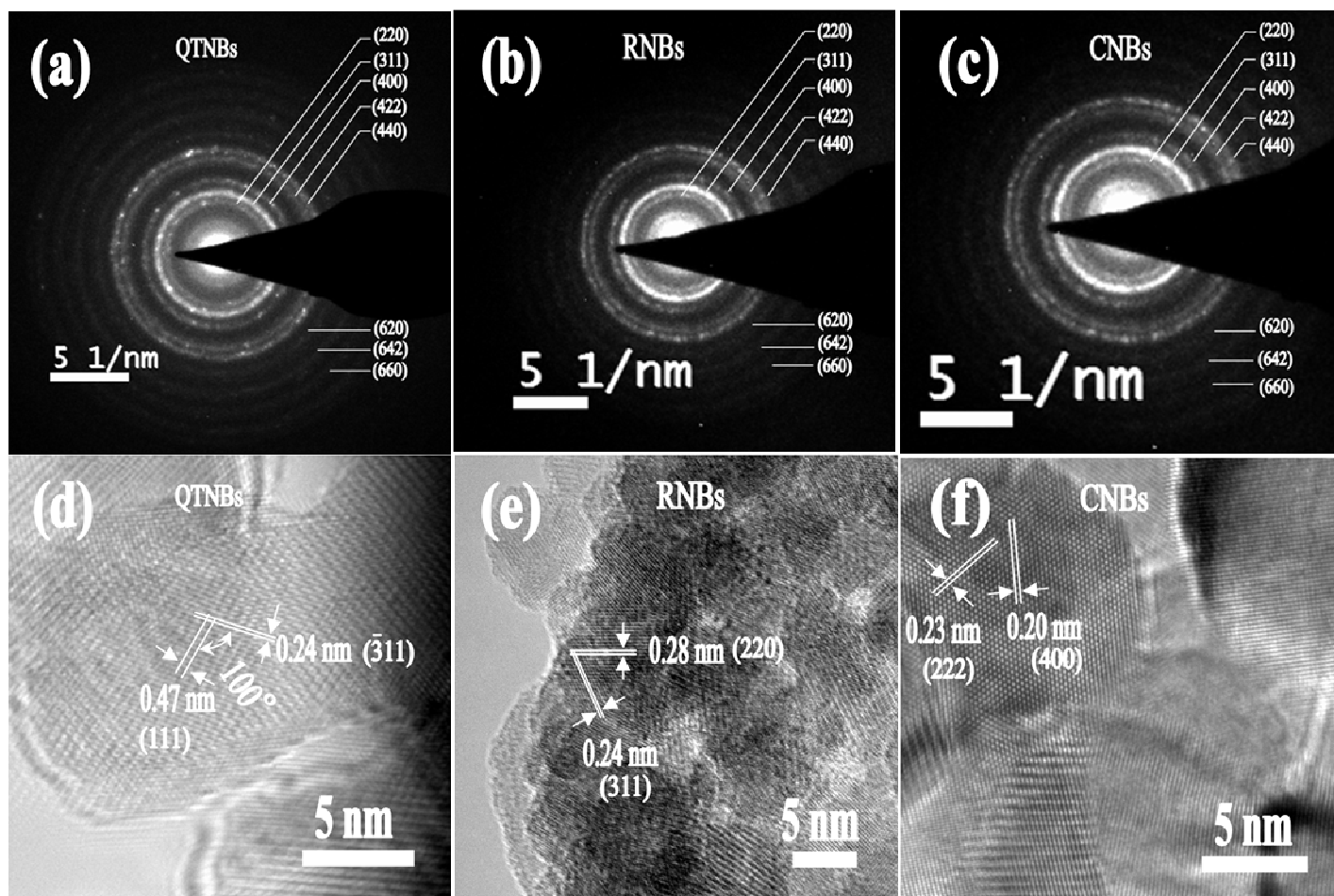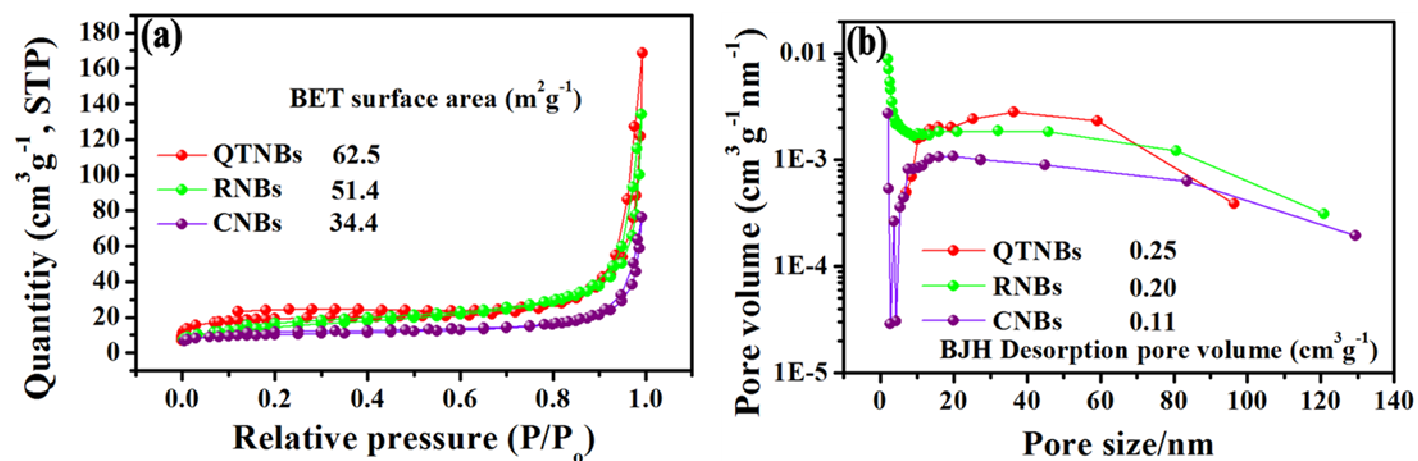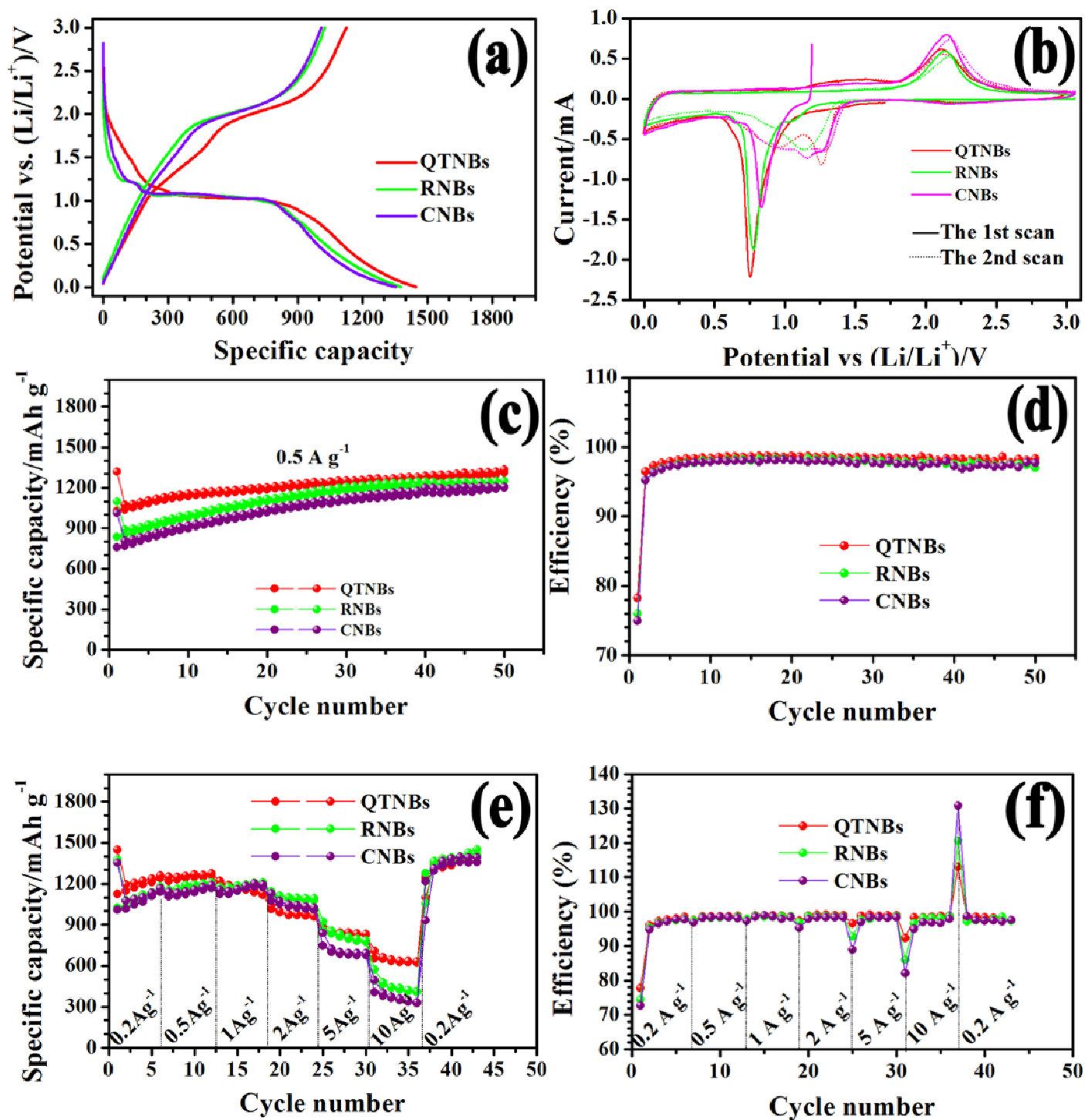
are the corresponding mapping images.

5

1

2 **Figure 4.** (a)-(c) SAED and (d)-(f) HRTEM images for the QTNBs, RNBs, and the CNBs respectively.

3

Figure 5. Surface and pore analysis for the various Co_3O_4 nanoboxes. (a) N_2 absorption-desorption isotherms.

(b) Distribution of the BJH desorption pore.

Figure 6. Electrochemical characterization for various Co_3O_4 nanoboxes: (a) the first charge-discharge curves, (b) typical cyclic voltammograms (CV), (c) cycling performance tested at 0.5 Ag^{-1}, (d) coulombic efficiency at 0.5 Ag^{-1}, (e) rate performance carried with altering rates from 0.2 Ag^{-1} to 10 Ag^{-1}, and (f) coulombic efficiency at variable rates from 0.2 Ag^{-1} to 10 Ag^{-1}.
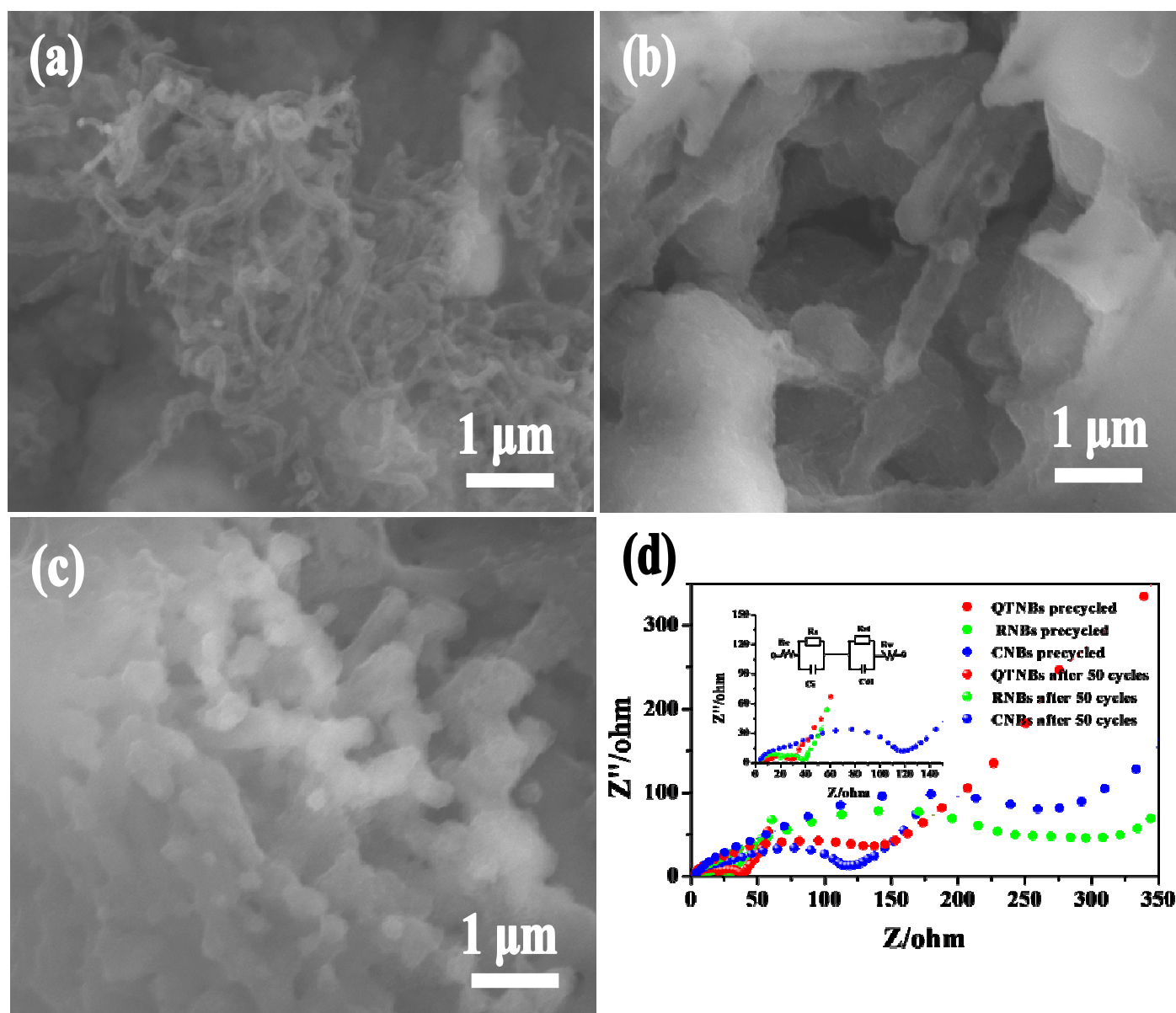
1
2　Figure 7 Ex-situ SEM images for various Co_3O_4 nanoboxes after 50 cycles: (a) QTNBs, (b) RNBs, and (c)

3　CNBs. (d) The electrochemical impedance spectra for various Co_3O_4 nanoboxes pre- and after 50 cycles.

Text

Excellent electrochemical properties were realized in quadrate Co_3O_4
nanoboxes derived from relevant coordination polymer nano-solids.

Color graphic